MATERIALS SCIENCE

Soft and ion-conducting hydrogel artificial tongue for astringency perception

Jeonghee Yeom*, Ayoung Choe*, Seongdong Lim†, Youngsu Lee, Sangyun Na, Hyunhyub Ko‡

Artificial tongues have been receiving increasing attention for the perception of five basic tastes. However, it is still challenging to fully mimic human tongue–like performance for tastes such as astringency. Mimicking the mechanism of astringency perception on the human tongue, we use a saliva-like chemiresistive ionic hydrogel anchored to a flexible substrate as a soft artificial tongue. When exposed to astringent compounds, hydrophobic aggregates form inside the microporous network and transform it into a micro/nanoporous structure with enhanced ionic conductivity. This unique human tongue–like performance enables tannic acid to be detected over a wide range (0.0005 to 1 wt %) with high sensitivity (0.292 wt $\%^{-1}$) and fast response time (~10 s). As a proof of concept, our sensor can detect the degree of astringency in beverages and fruits using a simple wipe-and-detection method, making a powerful platform for future applications involving humanoid robots and taste monitoring devices.

INTRODUCTION

A tongue is a muscular organ that is one of the softest, most flexible, and sensitive body parts in which thousands of mechanical receptors, taste receptors, and ion channels are located. The tongue is kept moist by a thin salivary film with a thickness of a few hundred micrometers (*1*), which is composed of 99% water and a mixture of electrolytes, immunoglobulins, and secretory proteins. Saliva plays a substantial role in the perception of tastes, where it dissolves tastants and enables them to bind to receptor cells or flow through ion channels more efficiently (*2*). Humans can sense and distinguish five basic tastes (sweet, sour, bitter, salty, and umami). Water-soluble tastants are perceived through taste receptor cells or ion channels via electrical signals generated from depolarization of the receptor cells upon binding of taste chemicals with receptors (sweet, bitter, and umami) or by the flow of sodium or hydrogen ions through the ion channels (salty and sour) (*3*).

Mimicking the sensing mechanisms of the human tongue, several artificial tongues have been developed based on lipid/polymer membranes (*4*, *5*), human taste receptors (*6*), or stripped epithelium cells (*7*). Among these strategies, a majority of artificial tongues developed for sensing the five basic tastes adopt specific target-binding systems that include aptamers (*8*), enzymes (*9*), or taste receptor–functionalized electronics (*6*) to achieve high selectivity and a low limit of detection. However, development of artificial tongues that fully emulate the sensing mechanism of astringency is still in the incipient stage, exhibiting poor performance, such as low selectivity and narrow detection range (*5*, *10*, *11*); the nature of astringency is derived from indirect stimulation of mechanoreceptors residing in the tongue upon complexation of ingested astringent foods and salivary film.

Astringency is stimulated by exposure to polyphenols, which are mainly found in unripe fruits, wines, and tea. Polyphenols are beneficial as strong antioxidant and anti-inflammatory substances (*12*), but they may also provoke negative nutritional impacts that can often be lethal when high doses are consumed (*13*). Astringency is perceived by the strong association of ingested astringent tastants and saliva proteins covering the tongue (*14*). When astringent tastants enter the oral cavity, they bind with secreted proteins to form insoluble precipitates on the tongue, resulting in shrinkage of the epithelium that causes dryness and a puckering feeling in the mouth. The unique sensing mechanism of astringency is based on indirect stimulation of mechanoreceptors residing in the ruptured salivary film, which consequently leads to the rare demonstration of artificial tongue for astringency based on specific target-binding methods. Moreover, to the best of our knowledge, demonstration of a fully flexible and soft artificial tongue that is highly selective to specific astringent tastants has not been achieved.

Here, mimicking the mechanism of human astringency perception, we introduce a soft hydrogel–based artificial tongue. Inspired by the thin salivary layer on the tongue, a soft and thin hydrogel film is integrated on a flexible polymer substrate through covalent bonding. The artificial tongue consists of mucin as secreted protein, lithium chloride (LiCl) as electrolyte, and polyacrylamide (PAAm) as the three-dimensional (3D) porous polymer network for the facile flow of electrolyte. The thickness of the soft hydrogel (200 μm) is comparable to that of an actual salivary layer on a human tongue; efficient adsorption and diffusion of astringent compounds inside the hydrogel occur. As a representative polyphenolic substance, tannic acid (TA) is used (*15*, *16*). When TA solution diffuses into the hydrogel matrix, incoming TA molecules bind and complex with the mucin to form hydrophobic aggregates and further transform the microporous hydrogel into the hierarchical micro/nanoporous structure, resulting in enhanced ionic conductivity. The artificial tongue exhibited a wide sensing range for TA [1 to 0.0005 weight % (wt %)], high sensitivity (0.292 wt $\%^{-1}$), and fast response time (~10 s). Furthermore, our flexible astringency sensors can detect the degree of astringency in real beverages and monitor the ripening of fruits using a simple wipe-and-detection method. In addition, the astringency sensor array acts as a portable taste mapping tool to detect degree of astringency and exposed location simultaneously.

Department of Energy Engineering, School of Energy and Chemical Engineering, Ulsan National Institute of Science and Technology (UNIST), Ulsan Metropolitan City 44919, Republic of Korea.
*These authors contributed equally to this work.
†Present address: Department of Materials, University of Oxford, Parks Road, Oxford OX1 3PH, UK.
‡Corresponding author. Email: hyunhko@unist.ac.kr

RESULTS

Astringency perception involves interaction between salivary protein and tannins. Tannins [e.g., TA, gallic acid (GA), and catechin (CAT)], which are a class of astringent polyphenols, form insoluble protein-tannin complexes through hydrogen bonding between hydroxyl groups of tannins and amide groups of proteins and hydrophobic interactions between aromatic rings of tannins and the hydrophobic domains of proteins (*10*, *16*). Binding processes induce protein-tannin complexes to be more compact and become larger via self-association. The resulting hydrophobic aggregates precipitate in the mouth and evoke oral dryness, which is responsible for the astringent taste. As a result, the ruptured salivary film stimulates mechanoreceptors and transmits signals to the brain to perceive astringency (Fig. 1A).

Inspired by the sensing mechanism of oral dryness caused by astringent tastants, we designed a soft hydrogel–based artificial tongue, which is a saliva-like ionic PAAm hydrogel containing mucin proteins and LiCl electrolytes (Fig. 1B). In the same manner as the human oral cavity, TA, a specific type of tannin, forms insoluble mucin-TA complexes through hydrophobic interactions between the aromatic rings of TA and hydrophobic amino acid domains of mucin, and hydrogen bonding of hydroxyl groups of TA with carbonyl and amide groups of mucin (*17*). Coupling between mucin and a sufficient number of phenolic hydroxyl groups of TA enables TA to surround mucin and generate hydrophobic mucin-TA complexes (dimers or trimers). Furthermore, self-association via hydrogen bonding leads to much larger hydrophobic aggregates inside the polymer matrix. During the complexation process, substantial tension is applied to the micropores, resulting in tearing off the original pore walls by the generation of hydrophobic linkages. These hydrophobic aggregates build up nanoporous structures inside the microporous hydrogel, ultimately facilitating efficient ion transport through the hierarchical micro/nanoporous structures. Figure 1 (C and D) shows that the microporous artificial tongue transforms to the hierarchical micro/nanoporous networks in response to TA, indicating that the mucin-TA complexes are homogeneously formed inside the porous hydrogel.

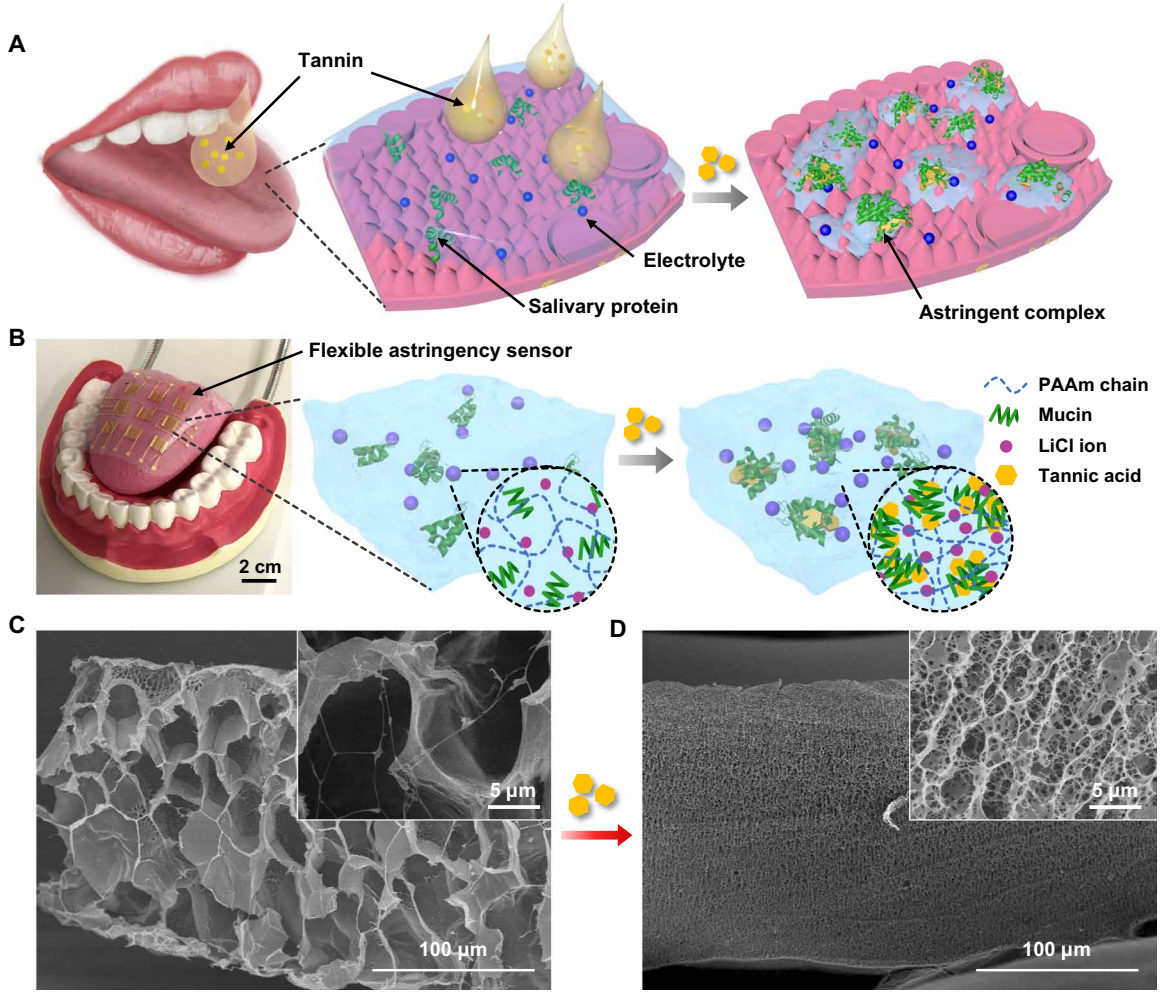

Fig. 1. Operating principle of the astringency detectable sensor. (**A**) Schematic illustration of astringency sensing principle of the human tongue. (**B**) Photograph of artificial tongue and schematic illustration of the astringency sensing principle of artificial tongue. Photo credit: J.Y., Ulsan National Institute of Science and Technology. (**C**) Scanning electron microscopy (SEM) image of the astringency detectable hydrogel before exposure to TA. (**D**) SEM images of the astringent detectable hydrogel after exposure to 1 wt % TA for 60 s; insets in (C) and (D) are magnified SEM images demonstrating micropores and micro/nanopores, respectively.

As schematically shown in Fig. 2A, mucin is a dumbbell-shaped protein where hydrophobic globules are linked on both sides of the highly glycosylated peptide backbone (*17*), mainly functioning as a lubricating mucus layer in the human body. When a large amount of mucin exists in the PAAm hydrogel, the hydrophobic globules cross-link with each other and form a mucin polymer through disulfide bonding between the unglycosylated regions (*17*, *18*). The mucin polymers are homogeneously integrated in the PAAm hydrogel network through physical entanglement, resulting in lumps randomly associated with the fibrillar structures (Fig. 2B). When the mucin polymer is mixed with TA, the formation of large mucin-TA precipitates leads to an increase in surface roughness (8.8 nm) compared with that of mucin (3.6 nm) as shown in fig. S1. The chemical composition and bonding of mucin and TA are observed by Fourier-transform infrared (FTIR) and Raman spectroscopies (Fig. 2, C and D). The characteristic vibrational peaks of mucin at 1644 and 1550 cm^{-1} correspond to the amide I and amide II bands of the protein, respectively (Fig. 2Ci) (*19*, *20*). In the presence of TA, the amide I and amide II bands shift to higher wave numbers (1650 and 1554 cm^{-1}) due to the change in backbone conformation of mucin after binding with TA, and an additional peak at 1718 cm^{-1} arises from the C=O groups of TA (Fig. 2Cii). The Raman spectra can provide additional structural information of mucin; the amide I band at 1657 cm^{-1} is mainly attributed to the stretching C=O of the peptide carbonyl groups, but after treatment with TA, the amide I band shifts to 1670 cm^{-1}, indicating secondary structure of the mucin is changed after mucin-TA complexation (Fig. 2D) (*21*, *22*). The additional peaks at 1609 and 1713 cm^{-1} are assigned to the aromatic C=C and C=O bonds of TA, respectively.

For fabrication of the artificial tongue, we designed a flexible chemiresistive sensor using a saliva-like hydrogel as an active layer on a flexible substrate. Since the incoming taste compounds are adsorbed and diffuse inside the artificial tongue, the hydrogel needs to be thin enough to attain a short diffusion time (*23*) while also being thick enough to prevent detrimental interference from external environmental factors. Furthermore, the interface between dissimilar hydrogel and electrode should be tight and conformal, which can be achieved through physical (*24*) or chemical bonding (*25*). Figure 3A illustrates the fabrication process of the artificial tongue. Poly (ethylene naphthalate) (PEN) is used as the flexible substrate owing to its chemical and thermal stability arising from the presence of two condensed aromatic rings. After oxygen plasma treatment, formation of polar hydroxyl and carboxylic groups makes PEN hydrophilic (*26*), which enables attachment of the saliva-like hydrogel on the substrate. To precisely control the thickness of the saliva-like hydrogel and create a tight interface between the electrode and hydrogel, direct ultraviolet (UV) polymerization of the hydrogel is performed on the substrate with the 3-(trimethoxysilyl)propyl methacrylate (TMSPMA),which is used as a chemical anchoring agent that allows covalent bonding of the hydrogel to the substrate (*25*). The silane groups of TMSPMA make hydrogen bondings with the hydroxyl and carboxylic groups of PEN, while the other end groups polymerize with the acrylate of the acrylamide chain in the PAAm hydrogel network, rendering a conformal interface between the hydrogel and electrode. The flexible electrode maintains stable electrical resistance (~4 ohms) for the bending distances ranging from 20 to 2 mm and multiple bending cycles over 500 times with a 2-mm bending distance (fig. S2).

Figure 3 (B and C) schematically illustrates the working principle of the artificial tongue under external astringency stimuli. Initially, the artificial salivary film exhibits moderate electrical conductivity due to the mobile LiCl ions inside the 3D microporous networks. The micropores are hydrophilic due to the presence of amide groups from polymer chains and mucin, which limits the flow of electrolyte. In this system, electrolytes stick to the hydrophilic micropores (no-slip boundary) due to electrostatic interactions between ions and the pore walls, resulting in poor ion transport (Fig. 3B). Once the artificial tongue is exposed to TA, complexation of mucin and TA generates hydrophobic nanochannels inside the microporous hydrogel and changes the interactions between electrolytes and the pore walls. The hydrophobic nanopores lead to the fast slip

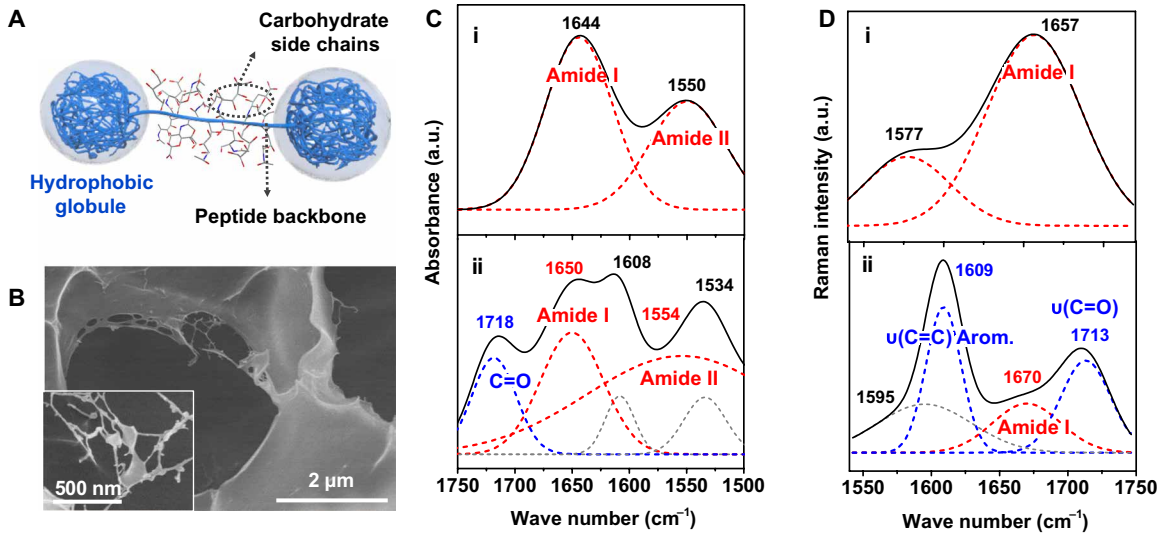

Fig. 2. Binding mechanism of mucin and TA. (**A**) Schematic illustration of mucin. (**B**) SEM image of the mucin polymer dispersed in the PAAm hydrogel network; inset image is magnified part of the pore edge. (**C**) FTIR spectra of (i) mucin and (ii) mixture of mucin and TA. (**D**) Raman spectra of (i) mucin and (ii) mixture of mucin and TA. a.u., arbitrary unit.

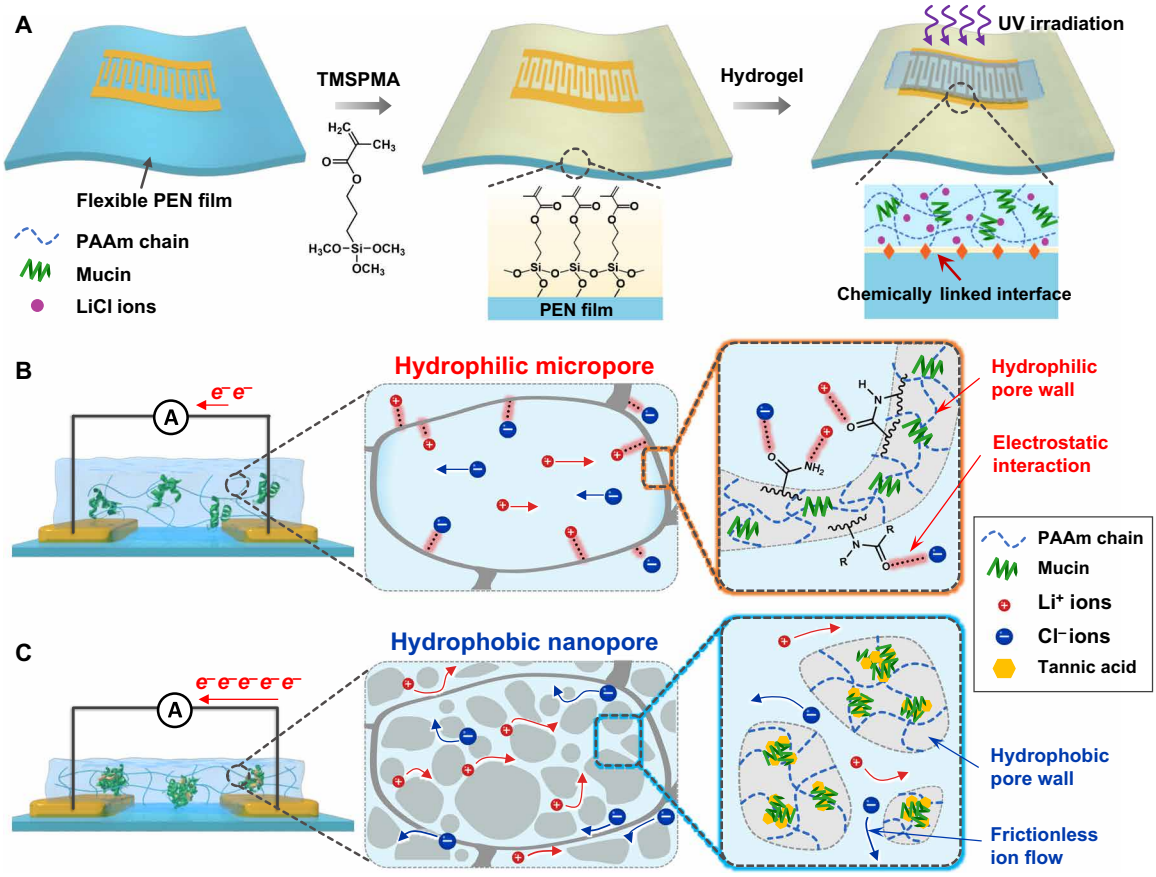

Fig. 3. Design of the flexible artificial tongue. (**A**) The fabrication process of the flexible astringency sensor. (**B**) Schematic illustration of the working principle of the astringency sensor before TA treatment (left); a hydrophilic micropore in the hydrogel (center); magnified pore walls visualizing the electrostatic interaction–limited ion flow (right). (**C**) Schematic illustration of the working principle of astringency sensor after TA treatment (left); a hierarchical micro/nanopore in the hydrogel (center); magnified pore walls of hydrophobic nanopore visualizing enhanced ion flow (right).

(or frictionless) flow of LiCl ions due to reduced electrostatic interactions, resulting in enhanced ion transport through the hierarchical porous structures (Fig. 3C) (*27*–*29*). Figure S3 exhibits the marked changes in the pore structure after treatment with TA. Initially, the artificial tongue has large micropores with average pore size of 16.7 μm (fig. S3, A and B). After TA treatment, the large micropores (16.7 μm) transform into hierarchical micro/nanoporous structures with smaller micropores (~1.3 μm) and nanopores (~211 nm), where the nanopores are newly generated due to the formation of hydrophobic mucin-TA linkages (fig. S3, C and D). In addition to the structural changes, the thickness of the artificial salivary film slightly decreases from 211 to 186 μm (fig. S4), indicating that the slight shrinkage is not a dominant factor on the sensing mechanism compared with the changes in the pore structures. The drastic formation of hydrophobic nanopores after TA treatment is a major contributor to the perception of astringency by increasing ionic conductivity.

To investigate the sensing performance of the artificial tongue, the relative current changes ($\Delta I/I_o$) are monitored under various concentrations of TAs (fig. S5). The current rapidly increases within 10 s and then saturates, indicating fast adsorption and diffusion of TA into the artificial tongue. While the artificial tongue is highly sensitive to TA, the ionic PAAm hydrogel without mucin shows poor sensitivity to TA (fig. S6A) due to the absence of the hydrophobic nanopore structures induced by the mucin-TA complex. The ionic PAAm hydrogel without mucin exhibits microporous structure even after TA treatment (fig. S6, B and C). The current changes ($\Delta I/I_o$) as a function of the concentration of TA are shown in Fig. 4A, which can be explained by an adsorption-dominated process following the empirical power-law curve of the adsorption isotherm given as $(\Delta I/I_o) = KC_{TA}{}^n$, where C_{TA} is the TA concentration, and K and n are the adsorption capacity and intensity, respectively (*30*, *31*). The exponent "n" obtained at 10, 30, and 60 s are 0.300, 0.297, and 0.281, showing all exponents less than 0.5, which indicates the adsorption of TA molecules in the hydrogel is favorable (fig. S7) (*32*). The adsorption isotherm increases rapidly at low concentrations and reaches saturated $\Delta I/I_o$ due to the limited number of adsorption sites. Surface-adsorbed TA molecules successively diffuse through the hydrogel pores and generate hydrophobic nanopores inside the micropores, resulting in enhanced ion transport through the hierarchical micro/nanoporous hydrogel.

The resulting artificial tongue has a wide sensing range (0.0005 to 1 wt %) and a linear sensitivity of 0.292 wt $\%^{-1}$ after 60 s of TA exposure when a logarithmic scale is adopted (fig. S8). Tables S1 and S2 summarize recent studies on the artificial tongue that detects various tastes (*4*–*7*, *10*, *33*). Until now, most research used human taste receptors (*6*, *33*) or taste epithelium cells (*7*) to achieve fast response time and notable sensing performance. However, it is impossible to apply such specific target-binding methods to detect

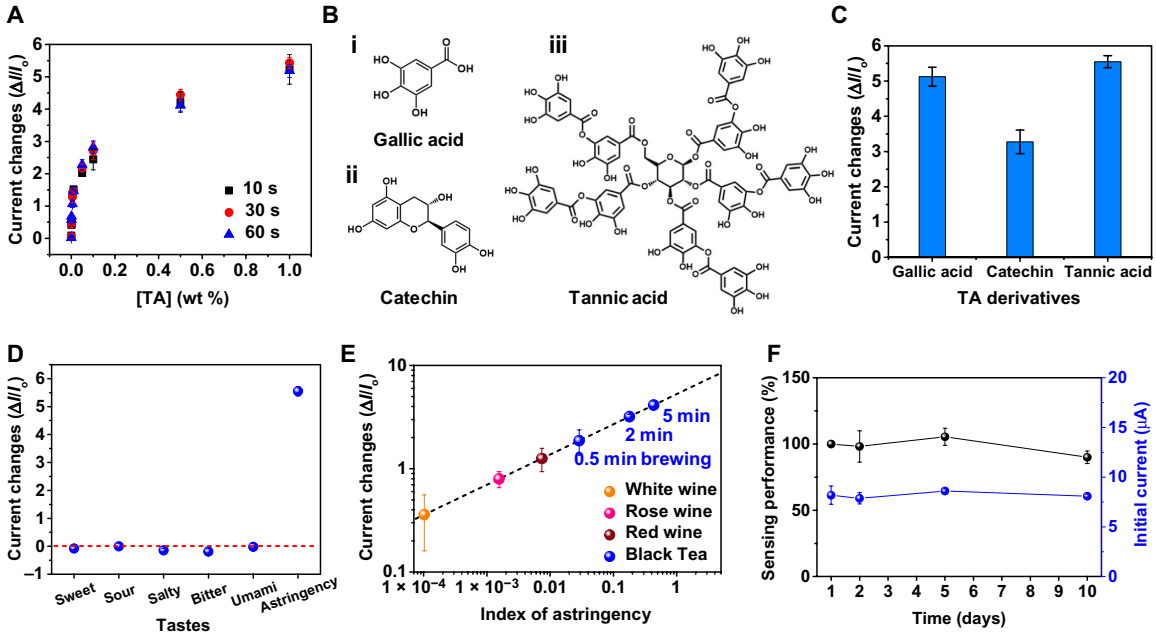

Fig. 4. Sensor performance of the artificial tongue. (**A**) Current changes ($\Delta I/I_o$) of the artificial tongue as a function of TA concentration. (**B**) Molecular structures of the polyphenolic derivatives: (i) GA, (ii) CAT, and (iii) TA. (**C**) Universal sensing capability of the artificial tongue under treatment with 5 mM of three different polyphenolic derivatives for 60 s. (**D**) Selective sensing performance of the artificial tongue toward the five basic tastes and astringency measured after exposure for 60 s; all tastants were 5 mM. (**E**) Astringency monitoring for real beverages: white wine, rose wine, red wine, and black tea leaves with different brewing times. (**F**) Long-term stability of the artificial tongue in terms of the sensing performance ($\Delta I/I_o$) × 100 (%) and the initial current (I_o). Values [(A) and (C) to (F)] represent means and SD from three to five samples.

astringent compounds, since astringency is not a receptor-binding sensation. Furthermore, the sensing ranges of specific binding systems are far below the human sensing threshold, indicating that they cannot be applicable for the practical fields, such as taste monitoring or neuroprosthetic devices for the taste blindness and standard index of tastes in food and pharmaceutical industries (table S2). Among nonspecific binding systems (*4*, *5*, *10*), our sensor exhibits a wide sensing range (2.9 to 5880 μM) that covers human sensing threshold (30 μM) and fast response time (~10 s) without adopting real taste cells or a sophisticated fabrication process. Although a miniaturized astringency sensor was developed using lipid/polymer membranes (*5*), it had a narrow sensing range, required a preliminary calibration process, and was also rigid rather than flexible. Overall, our sensor is advantageous in terms of facile fabrication, flexibility, no need for precalibration, wide sensing range, and fast response time comparable to sensors using real taste cells.

To elucidate the reliability of the artificial tongue, relative current changes of two unknown TA solutions were measured and plotted on the linearly fitted current change graph, resulting in TA concentrations of 0.179 and 0.0193 wt % (fig. S9A). UV–visible (vis) absorbance measurements at 377 nm of five TA solutions (0.001, 0.01, 0.1, 0.5, and 1 wt %) were fitted linearly and used to verify the concentrations of the unknown TA solutions, considering that the absorbance intensity is proportional to the concentration of analyte present (fig. S9, B and C). Analysis of the absorbance intensity of unknown TAs shows that their concentrations can be calculated as 0.185 and 0.0207 wt % (fig. S9D). These results only deviate by 0.42 and 0.10% from the values determined with the artificial tongue, demonstrating that the artificial tongue is highly accurate over a wide detection range.

In addition to TA, our artificial tongue can detect other types of small polyphenolic derivatives. As shown in Fig. 4Bi and ii, GA and CAT are types of polyphenolic acids with lower molecular weight than TA (Fig. 4Biii). Relative current changes of GA, CAT, and TA were measured at the same concentration (5 mM) after exposure for 60 s. Figure 4C shows that the astringency sensor is capable of detecting various polyphenolic derivatives since mucin can also bind to other polyphenolic compounds and form complexes. In the case of CAT, it shows ~60% of the current changes compared with GA and TA, since GA and TA have larger kinetic association constants and smaller kinetic dissociation constants than CAT (*34*), reflecting a stronger interaction between mucin and GA/TA than CAT. In addition, our artificial tongue provides high selectivity for the astringent taste over the other five basic tastants (sweet, sour, salty, bitter, and umami) since the five basic taste molecules do not interact with mucin inside the artificial tongue (Fig. 4D). In this test, the same concentrations (5 mM) of glucose, citric acid, sodium chloride, quinine, and glutamic acid are used for the representative sweet, sour, salty, bitter, and umami tastants, respectively. The interaction between mucin and the tastants can also be observed through changes in the porous structures. In the case of polyphenolic compounds (TA, GA, and CAT), hierarchical micro/nanopores are observed, whereas microporous structures are maintained for the other five basic tastants (fig. S10).

On the basis of the universal sensing capability for various astringent tastants and selectivity from five basic tastes, our artificial tongue offers potential for utilization as a standard index of astringency in practical sensing applications, such as detecting and standardizing astringency in real astringent beverages (Fig. 4E). For astringency evaluation of real beverages, three different types of wines (red, rose, and white) and black tea with different brewing times were used as the sensing materials. In the same manner as the detection of TA solutions, the degree of astringency in beverages can be determined by monitoring specific current changes ($\Delta I/I_o$) and fitting on the graph

of standard astringency. The characteristic difference of red, rose, and white wines comes from the amount of astringent tastants in grape seeds and skins during wine production. Red wine exhibits the highest degree of astringency since it is fermented using whole grapes with skins and seeds, which contain a large amount of tannins (*35*). The amount of skins and seeds of grapes decreases in rose wine and is almost absent for white wine, resulting in reduced astringency for rose wine and a minute degree of astringency in white wine. In addition, black tea leaves were brewed for 0.5, 2, and 5 min to infuse astringent compounds, which show a stepwise increase in astringency according to the brewing time.

For real-world applications, it is necessary to consider the stability of the sensors. However, traditional hydrogels are mostly filled with water, causing dehydration under ambient conditions as time goes by. To overcome this issue, hydrogels were encapsulated with elastomers (*36*), which cannot be applied in the artificial tongue due to the limited transport of tastants through the elastomer and inside the active matrix. Instead, LiCl is adopted in our artificial tongue, which functions as both a conductive and hydrating agent. LiCl prevents dehydration of the hydrogel even for a long duration since LiCl salts can efficiently decrease vapor pressure by formation of hydrated ions (*37*). The artificial tongue is fully functional when it is kept under ambient conditions [25°C, 60% relative humidity (RH)] over 10 days without storing devices in LiCl solution (Fig. 4F). In addition, our artificial tongue exhibits stable sensing performances over a broad sensing temperature range. When the artificial tongue is treated with TA (1 wt %) solution with different temperatures from 25 to 65°C for 10 to 60 s (fig. S11), the artificial tongue exhibits highly stable sensing performances even at 65°C for 10 to 30 s and maintained 88% of original sensing performance at 65°C for 60 s. The broad sensing temperature range of our artificial tongue is attributed to the highly glycosylated backbone of mucin. The large amount of polysaccharide moiety bound to the backbone leads to the remarkable thermal and kinetic stability of mucin (*38*, *39*).

Humans can perceive tastes by licking the liquid residue on the surface of solid foods by using the flexible tongue (Fig. 5A). However, previous artificial tongues show limited detection of trace amounts of analytes since a bulk liquid bath for the electrochemical reaction and preliminary dissolution of analytes are required before the measurement. In addition, those sensors were hardly able to wipe and detect a small amount of tastants due to the rigidity and bulkiness of the sensor systems. On the other hand, our astringency sensor can directly analyze liquid analytes on curved solid surfaces without any advanced preparations, enabling a wipe-and-detection method for tastants by bending and wiping the sensor device (Fig. 5A). Unripe fruits have a high content of polyphenolic compounds, making the fruits astringent. Among them, unripe persimmon contains a large amount of water-soluble tannin, evoking an astringent taste. During the ripening process, the water-soluble tannin becomes a water-insoluble tannin due to polymerization and condensation of tannins, resulting

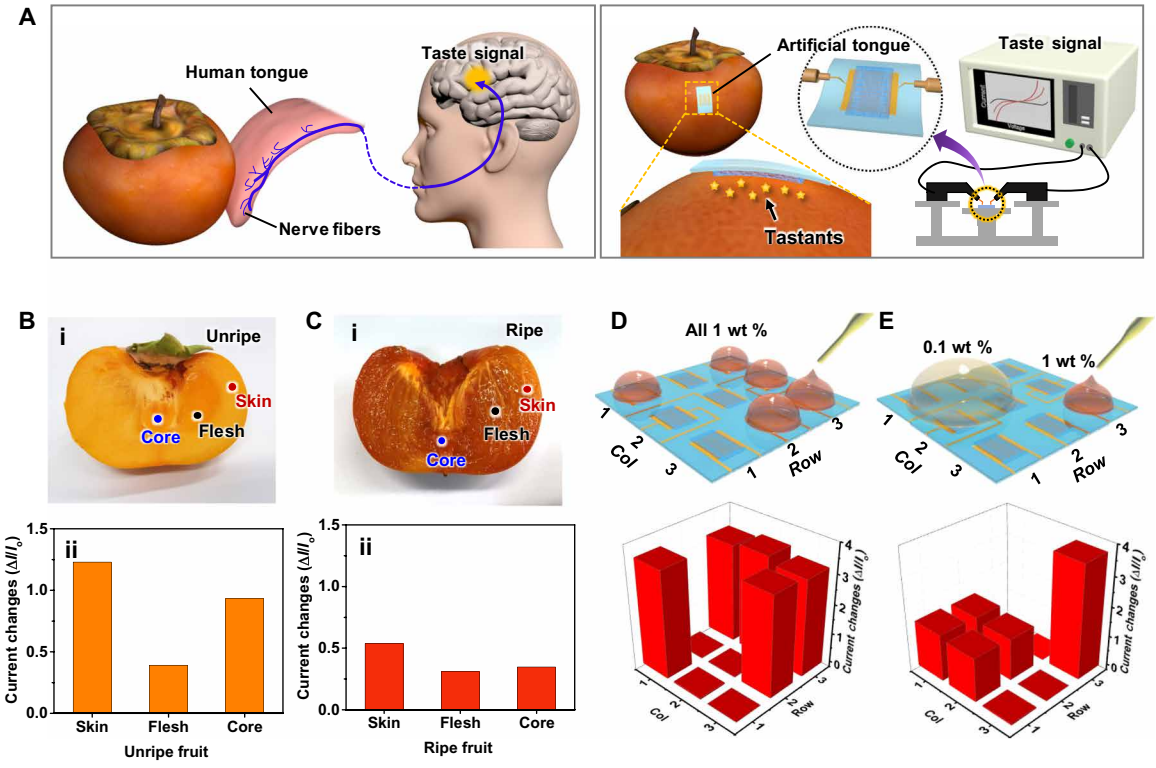

Fig. 5. Applications of the artificial tongue. (**A**) Schematic illustration of wipe-and-detection of the human tongue and artificial tongue. (**B**) Astringency detection of an unripe persimmon: (i) photograph of unripe persimmon and (ii) current changes at different parts of the unripe persimmon. Photo credit: J.Y., Ulsan National Institute of Science and Technology. (**C**) Astringency detection of a ripe persimmon: (i) photograph of ripe persimmon and (ii) current changes at different parts of the ripe persimmon. Photo credit: J.Y., Ulsan National Institute of Science and Technology. (**D**) Scheme of the arrayed artificial tongue with five drops of 1 wt % TA and resulting taste mapping of the arrayed artificial tongue. (**E**) Scheme of the arrayed artificial tongue with 0.1 and 1 wt % of TA and corresponding taste mapping data; the size of sensing elements for taste mapping (D and E) is 6 × 10 mm for each pixel.

in nonastringent persimmons (*40*). Our artificial tongue can visualize the degree of astringency in different regions of unripe persimmon by wiping on various parts of the fruit, such as core, flesh, and skin (Fig. 5Bi). As shown in Fig. 5Bii, a higher degree of astringency is observed when the artificial tongue is attached to the skin and core, while flesh shows relatively low astringency (*37*). When the persimmon is ripe, the core, flesh, and skin exhibit reduced astringency due to the formation of insoluble tannins during ripening (Fig. 5C). In addition, we fabricated a flexible artificial tongue with a 3 × 3 array (fig. S12). The astringency sensor array can be used as a portable taste mapping device. When 1 wt % of TA solution is applied on the five different spots of the array, the sensor can provide taste mapping through corresponding current changes on the specific regions (Fig. 5D). Likewise, two different TAs (1 and 0.1 wt %) were also treated on the taste sensor array (Fig. 5E), demonstrating different current changes on each spot, which proves simultaneous detection of the degree of astringent compounds and treated spots.

DISCUSSION

In this work, we presented an artificial tongue that is fully inspired from the human sensing mechanism. The artificial tongue can be prepared by facile UV polymerization on a flexible substrate and exhibit extraordinary sensing capabilities, such as a wide sensing range and a low limit of detectable concentration and high selectivity from other tastes. Upon exposure to astringent compounds, the microporous hydrogel is converted into micro/nanoporous structures, resulting in shortened diffusion paths of the electrolytes, as well as frictionless flow of electrolyte due to the hydrophobic nature of the nanopores to increase the flow rate of ions. Further optimization of the proteins can improve the universal sensing capability regardless of various types of polyphenolic derivatives as well as enhanced sensing performance with negligible errors. The outstanding results of the astringent sensor could pave the way to develop soft artificial tongues for astringency sensing, making it attractive to apply into various applications, such as an astringency indicator for taste quantification/evaluation, studies of taste disorders, and humanoid robots.

MATERIALS AND METHODS

Fabrication of the hydrogel-based artificial tongue

The hydrogel was synthesized using acrylamide (AAm; Sigma-Aldrich, A8887) as monomers, mucin from porcine stomach (Sigma-Aldrich, M1778), LiCl (Sigma-Aldrich, 310468), *N*,*N*′-methylenebisacrylamide (BIS; Sigma-Aldrich, 146072) as a cross-linker, and 2,2-diethoxyacetophenone (DEAP; Sigma-Aldrich, 227102) as a photoinitiator. The artificial tongue was prepared by dissolving AAm (1 M) in 1 M LiCl solution. And 1 wt % of BIS was added with respect to the weight of AAm to cross-link the hydrogel. After fully dispersing mucin (20 mg/ml) in the pregel solution in an ice bath, DEAP was added, and nitrogen was bubbled through the pregel solution to remove dissolved oxygen for 7 min.

Bonding hydrogel on the PEN film

For bonding of the PAAm-based hydrogel on the PEN film, the interdigitated electrode evaporated PEN substrates (Teijin DuPont Films) were treated with oxygen plasma for 3 min to generate hydrophilic surface functional groups on the film. Then, PEN substrates were immersed in the TMSPMA (Sigma-Aldrich, 440159) solution for 3 min to silanize the substrates. The TMSPMA solution was prepared by adding 1 ml of TMSPMA in 200 ml of ethanol and subsequent addition of 6 ml of acetic acid [10% (v/v) in water] under gentle stirring. After surface functionalization, the PEN substrate was washed thoroughly with ethanol and dried under a stream of nitrogen gas. Thereafter, the pregel solution was polymerized under UV irradiation (365 nm, 15 W) for 25 min on the functionalized PEN substrates. The polymerized gel was immersed in the same concentration of LiCl batch overnight to absorb LiCl solution and reach equilibrium state.

Characterization

The cross-sectional morphology of the artificial tongue was examined by a field emission scanning electron microscope (S-4800, Hitachi). The thickness of the artificial tongue was measured using an optical microscope (BX53, Olympus). The molecular interaction of mucin and TA was determined by an FTIR spectrometer (670/620, Varian) and a confocal Raman microscope (alpha300R, WITec). The current change of the artificial tongue was measured by a semiconductor characterization system (4200, Keithley Instruments) and a probe station (8000, MS Tech). The roughness of mucin and the mucin-TA complex was determined by an atomic force microscope (DI-3100, Veeco). The bending stability of the Au/PEN film was measured using a bending tester (JIBT-200, Junil Tech). The UV-vis absorbance of TA solution was measured by a UV–vis–NIR (near infrared) spectrophotometer (Cary 5000, Agilent).

SUPPLEMENTARY MATERIALS

Supplementary material for this article is available at http://advances.sciencemag.org/cgi/content/full/6/23/eaba5785/DC1

REFERENCES AND NOTES

1. L. M. Collins, C. Dawes, The surface area of the adult human mouth and thickness of the salivary film covering the teeth and oral mucosa. *J. Dent. Res.* **66**, 1300–1302 (1987).
2. R. Matsuo, Role of saliva in the maintenance of taste sensitivity. *Crit. Rev. Oral Biol. Med.* **11**, 216–229 (2000).
3. E. R. Kandel, J. H. Schwartz, T. M. Jessell, S. A. Siegelbaum, A. J. Hudspeth, in *Principles of Neural Science* (McGraw-Hill New York, 2000), vol. 4.
4. X. Wu, H. Onitake, Z. Huang, T. Shiino, Y. Tahara, R. Yatabe, H. Ikezaki, K. Toko, Improved durability and sensitivity of bitterness-sensing membrane for medicines. *Sensors* **17**, 2541 (2017).
5. Y. Tahara, A. Ikeda, Y. Maehara, M. Habara, K. Toko, Development and evaluation of a miniaturized taste sensor chip. *Sensors* **11**, 9878–9886 (2011).
6. S. R. Ahn, J. H. An, H. S. Song, J. W. Park, S. H. Lee, J. H. Kim, J. Jang, T. H. Park, Duplex bioelectronic tongue for sensing umami and sweet tastes based on human taste receptor nanovesicles. *ACS Nano* **10**, 7287–7296 (2016).
7. Q. Liu, D. Zhang, F. Zhang, Y. Zhao, K. J. Hsia, P. Wang, Biosensor recording of extracellular potentials in the taste epithelium for bitter detection. *Sens. Actuators B* **176**, 497–504 (2013).
8. C. Wu, L. Du, L. Zou, L. Huang, P. Wang, A biomimetic bitter receptor-based biosensor with high efficiency immobilization and purification using self-assembled aptamers. *Analyst* **138**, 5989–5994 (2013).
9. W. Gao, S. Emaminejad, H. Y. Y. Nyein, S. Challa, K. Chen, A. Peck, H. M. Fahad, H. Ota, H. Shiraki, D. Kiriya, D.-H. Lien, G. A. Brooks, R. W. Davis, A. Javey, Fully integrated wearable sensor arrays for multiplexed in situ perspiration analysis. *Nature* **529**, 509–514 (2016).
10. S. Ma, H. Lee, Y. Liang, F. Zhou, Astringent mouthfeel as a consequence of lubrication failure. *Angew. Chem. Int. Ed. Engl.* **55**, 5793–5797 (2016).
11. J. Horne, J. Hayes, H. T. Lawless, Turbidity as a measure of salivary protein reactions with astringent substances. *Chem. Senses* **27**, 653–659 (2002).
12. H. Zhang, R. Tsao, Dietary polyphenols, oxidative stress and antioxidant and anti-inflammatory effects. *Curr. Opin. Food Sci.* **8**, 33–42 (2016).
13. K.-T. Chung, T. Y. Wong, C.-I. Wei, Y.-W. Huang, Y. Lin, Tannins and human health: A review. *Crit. Rev. Food Sci. Nutr.* **38**, 421–464 (1998).
14. M. R. Bajec, G. J. Pickering, Astringency: Mechanisms and perception. *Crit. Rev. Food Sci. Nutr.* **48**, 858–875 (2008).

15. A. Troszyńska, O. Narolewska, S. Robredo, I. Estrella, T. Hernández, G. Lamparski, R. Amarowicz, The effect of polysaccharides on the astringency induced by phenolic compounds. *Food Qual. Prefer.* **21**, 463–469 (2010).
16. R. Xu, S. Ma, P. Lin, B. Yu, F. Zhou, W. Liu, High strength astringent hydrogels using protein as the building block for physically cross-linked multi-network. *ACS Appl. Mater. Interfaces* **10**, 7593–7601 (2018).
17. G. E. Yakubov, A. Papagiannopoulos, E. Rat, R. L. Easton, T. A. Waigh, Molecular structure and rheological properties of short-side-chain heavily glycosylated porcine stomach mucin. *Biomacromolecules* **8**, 3467–3477 (2007).
18. T. A. Waigh, A. Papagiannopoulos, A. Voice, R. Bansil, A. P. Unwin, C. D. Dewhurst, B. Turner, N. Afdhal, Entanglement coupling in porcine stomach mucin. *Langmuir* **18**, 7188–7195 (2002).
19. M. C. Chang, J. Tanaka, FT-IR study for hydroxyapatite/collagen nanocomposite cross-linked by glutaraldehyde. *Biomaterials* **23**, 4811–4818 (2002).
20. P. Lasch, M. Boese, A. Pacifico, M. Diem, FT-IR spectroscopic investigations of single cells on the subcellular level. *Vib. Spectrosc.* **28**, 147–157 (2002).
21. R. Tuma, Raman spectroscopy of proteins: From peptides to large assemblies. *J. Raman Spectrosc.* **36**, 307–319 (2005).
22. L. Ashton, P. D. A. Pudney, E. W. Blanch, G. E. Yakubov, Understanding glycoprotein behaviours using Raman and Raman optical activity spectroscopies: Characterising the entanglement induced conformational changes in oligosaccharide chains of mucin. *Adv. Colloid Interface Sci.* **199-200**, 66–77 (2013).
23. J. Li, D. J. Mooney, Designing hydrogels for controlled drug delivery. *Nat. Rev. Mater.* **1**, 16071–16087 (2016).
24. D. Wirthl, R. Pichler, M. Drack, G. Kettlguber, R. Moser, R. Gerstmayr, F. Hartmann, E. Bradt, R. Kaltseis, C. M. Siket, S. E. Schausberger, S. Hild, S. Bauer, M. Kaltenbrunner, Instant tough bonding of hydrogels for soft machines and electronics. *Sci. Adv.* **3**, e1700053 (2017).
25. H. Yuk, T. Zhang, S. Lin, G. A. Parada, X. Zhao, Tough bonding of hydrogels to diverse non-porous surfaces. *Nat. Mater.* **15**, 190–196 (2016).
26. E. Gonzalez, M. D. Barankin, P. C. Guschl, R. F. Hicks, Remote atmospheric-pressure plasma activation of the surfaces of polyethylene terephthalate and polyethylene naphthalate. *Langmuir* **24**, 12636–12643 (2008).
27. M. Majumder, N. Chopra, B. J. Hinds, Mass transport through carbon nanotube membranes in three different regimes: Ionic diffusion and gas and liquid flow. *ACS Nano* **5**, 3867–3877 (2011).
28. D. C. Tretheway, C. D. Meinhart, Apparent fluid slip at hydrophobic microchannel walls. *Phys. Fluids* **14**, L9–L12 (2002).
29. T. W. Allen, S. Kuyucak, S.-H. Chung, The effect of hydrophobic and hydrophilic channel walls on the structure and diffusion of water and ions. *J. Chem. Phys.* **111**, 7985–7999 (1999).
30. H. Ko, S. Chang, V. V. Tsukruk, Porous substrates for label-free molecular level detection of nonresonant organic molecules. *ACS Nano* **3**, 181–188 (2008).
31. P. S. Ghosal, A. K. Gupta, Development of a generalized adsorption isotherm model at solid-liquid interface: A novel approach. *J. Mol. Liq.* **240**, 21–24 (2017).
32. A. Bera, T. Kumar, K. Ojha, A. Mandal, Adsorption of surfactants on sand surface in enhanced oil recovery: Isotherms, kinetics and thermodynamic studies. *Appl. Surf. Sci.* **284**, 87–99 (2013).
33. S. R. Ahn, J. H. An, I. H. Jang, W. Na, H. Yang, K. H. Cho, S. H. Lee, H. S. Song, J. Jang, T. H. Park, High-performance bioelectronic tongue using ligand binding domain T1R1 VFT for umami taste detection. *Biosens. Bioelectron.* **117**, 628–636 (2018).
34. J. Gombau, P. Nadal, N. Canela, S. Gómez-Alonso, E. García-Romero, P. Smith, I. Hermosín-Gutiérrez, J. M. Canals, F. Zamora, Measurement of the interaction between mucin and oenological tannins by surface plasmon resonance (SPR); relationship with astringency. *Food Chem.* **275**, 397–406 (2019).
35. M. He, H. Tian, X. Luo, X. Qi, X. Chen, Molecular progress in research on fruit astringency. *Molecules* **20**, 1434–1451 (2015).
36. H. Yuk, T. Zhang, G. A. Parada, X. Liu, X. Zhao, Skin-inspired hydrogel–elastomer hybrids with robust interfaces and functional microstructures. *Nat. Commun.* **7**, 12028–12038 (2016).
37. Y. Bai, B. Chen, F. Xiang, J. Zhou, H. Wang, Z. Suo, Transparent hydrogel with enhanced water retention capacity by introducing highly hydratable salt. *Appl. Phys. Lett.* **105**, 151903–151907 (2014).
38. D. Shental-Bechor, Y. Levy, Effect of glycosylation on protein folding: A close look at thermodynamic stabilization. *Proc. Natl. Acad. Sci. U.S.A.* **105**, 8256–8261 (2008).
39. J. B. Madsen, K. I. Pakkanen, S. Lee, Thermostability of bovine submaxillary mucin (BSM) in bulk solution and at a sliding interface. *J. Colloid Interface Sci.* **424**, 113–119 (2014).
40. T. Tanaka, R. Takahashi, I. Kouno, G.-i. Nonaka, Chemical evidence for the de-astringency (insolubilization of tannins) of persimmon fruit. *J. Chem. Soc. Perkin Trans.* **1**, 3013–3022 (1994).

Acknowledgments

Funding: This work was supported by the National Research Foundation (NRF) of Korea (2018R1A2A1A05079100 and 2017M1A2A2087833). **Author contributions:** H.K. conceived the project. J.Y. designed the experiments and fabricated the devices. J.Y. and A.C. performed measurements, characterizations, and analysis. S.L. and Y.L. aided in the electrical characterizations and analysis of the sensor. S.N. aided in the fabrication of the sensor. H.K., J.Y., and A.C. wrote the paper, to which all authors provided feedback. **Competing interests:** The authors declare that they have no competing interests. **Data and materials availability:** All data needed to evaluate the conclusions in the paper are present in the paper and/or the Supplementary Materials. Additional data related to this paper may be requested from the authors.

Submitted 15 December 2019
Accepted 15 April 2020
Published 5 June 2020
10.1126/sciadv.aba5785

Citation: J. Yeom, A. Choe, S. Lim, Y. Lee, S. Na, H. Ko, Soft and ion-conducting hydrogel artificial tongue for astringency perception. *Sci. Adv.* **6**, eaba5785 (2020).

Science Advances

Soft and ion-conducting hydrogel artificial tongue for astringency perception

Jeonghee Yeom, Ayoung Choe, Seongdong Lim, Youngsu Lee, Sangyun Na and Hyunhyub Ko

Sci Adv **6** (23), eaba5785.
DOI: 10.1126/sciadv.aba5785